

# Soft Matter

Accepted Manuscript



This is an *Accepted Manuscript*, which has been through the Royal Society of Chemistry peer review process and has been accepted for publication.

*Accepted Manuscripts* are published online shortly after acceptance, before technical editing, formatting and proof reading. Using this free service, authors can make their results available to the community, in citable form, before we publish the edited article. We will replace this *Accepted Manuscript* with the edited and formatted *Advance Article* as soon as it is available.

You can find more information about *Accepted Manuscripts* in the [Information for Authors](#).

Please note that technical editing may introduce minor changes to the text and/or graphics, which may alter content. The journal's standard [Terms & Conditions](#) and the [Ethical guidelines](#) still apply. In no event shall the Royal Society of Chemistry be held responsible for any errors or omissions in this *Accepted Manuscript* or any consequences arising from the use of any information it contains.

# Dynamics of Self-Propelled Particles Under Strong Confinement

Yaouen Fily,<sup>\*a</sup> Aparna Baskaran,<sup>a</sup> Michael F. Hagan<sup>a</sup>

Received Xth XXXXXXXXXX 20XX, Accepted Xth XXXXXXXXXX 20XX

First published on the web Xth XXXXXXXXXX 20XX

DOI: 10.1039/b000000x

We develop a statistical theory for the dynamics of non-aligning, non-interacting self-propelled particles confined in a convex box in two dimensions. We find that when the size of the box is small compared to the persistence length of a particle's trajectory (strong confinement), the steady-state density is zero in the bulk and proportional to the local curvature on the boundary. Conversely, the theory may be used to construct the box shape that yields any desired density distribution on the boundary, thus offering a general tool to understand and design such confinements. When the curvature variations are small, we also predict the distribution of orientations at the boundary and the exponential decay of pressure as a function of box size recently observed in simulations in a spherical box.

## 1 Introduction

Active fluids consisting of self-propelled units are found in biology on scales ranging from the dynamically reconfigurable cell cytoskeleton<sup>1</sup> to swarming bacterial colonies<sup>2,3</sup>, healing tissues<sup>4,5</sup>, and flocking animals<sup>6</sup>. Experiments have begun to achieve the extraordinary capabilities and emergent properties of these biological systems in nonliving active fluids of self-propelled particles, consisting of chemically<sup>7–12</sup> or electrically<sup>13</sup> propelled colloids, or monolayers of vibrated granular particles<sup>14–16</sup>.

In contrast to thermal motion, active motion is correlated over experimentally accessible time and length scales. When the persistence length of active motion becomes comparable to the mean free path, uniquely active effects arise that transcend the thermodynamically allowed behaviors of equilibrium systems, including giant number fluctuations and spontaneous flow<sup>3,14,16–30</sup>. Importantly, a sufficient active persistence length is the only requirement for macroscopic manifestations of activity, as revealed by athermal phase separation of non-aligning, repulsive self-propelled particles<sup>31–41</sup>.

When boundaries and obstacles are patterned on the scale of the active correlation length, they dramatically alter the dynamics of the system, and striking macroscopic properties emerge<sup>42–52</sup>; for example, ratchets and funnels drive spontaneous flow in active fluids<sup>42,43,46–48</sup>. This effect has been used to direct bacterial motion<sup>53</sup> and harness bacterial power to propel microscopic gears<sup>54–56</sup>. However, optimizing such devices for technological applications requires understanding the interaction of an active fluid with boundaries of arbitrary shape. More generally, any real-world device necessarily includes boundaries, and thus the effects of bound-

ary size and shape are essential design parameters. Although recent studies have explored confinement in simple geometries<sup>43,44,51,52,57–62</sup>, there is no general theory for the effect of boundary shape.

In this paper, we study the dynamics of non-aligning and non-interacting self-propelled particles confined to two-dimensional convex containers, such as ellipses and polygons. We find that the boundary shape dramatically affects the active fluid's dynamics and thermomechanical properties in the limit of “strong confinement”, in which the container size is small compared to the active persistence length (the distance a particle travels before its orientation decorrelates). In particular: (i) particles are confined to the boundary, (ii) the steady-state distribution of particles at the boundary is proportional to the local curvature (see Fig. 1), and (iii) when the curvature varies slowly, the local pressure exerted on the boundary decays exponentially with the ratio of the radius of curvature to the active persistence length. Results (i) and (ii) are derived in the limit of small and slowly varying curvature radius, then extended to polygonal boxes. They likely hold for arbitrary convex boundaries, although the definition of “strong confinement” depends on the type of boundary. Together, these three results demonstrate that the boundary shape in an active system can sensitively control the behavior of particles within, and they constitute a first step in a theoretical framework to design confinement geometries that give rise to specific material properties or device functionalities.

## 2 Model

We consider an overdamped self-propelled particle with position  $\mathbf{r}$  and orientation  $\hat{\mathbf{v}} = \cos \theta \hat{\mathbf{x}} + \sin \theta \hat{\mathbf{y}}$  whose dynamics is

<sup>a</sup> Martin A. Fisher School of Physics, Brandeis University, Waltham, MA 02454, USA

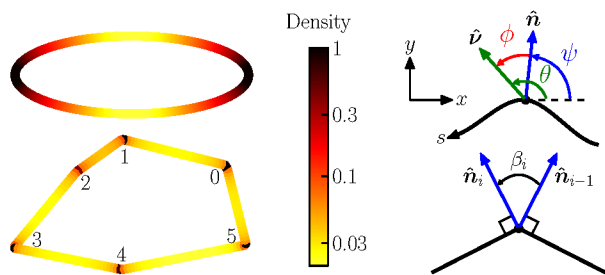


**Fig. 1** Left: Visual summary of simulation results showing particles concentrated in high curvature regions. Right: Geometric notations for the analytic theory for a smooth boundary (top) and a polygon (bottom).

described by

$$\dot{\mathbf{r}} = v_0 \hat{\mathbf{v}} + \mu \mathbf{F}_{\text{wall}}, \quad \dot{\theta} = \xi(t) \quad (1)$$

where  $v_0$  is the self-propulsion speed,  $\mu$  is the mobility,  $\xi$  is a white Gaussian noise with zero mean and correlations  $\langle \xi(t) \xi(t') \rangle = 2D_r \delta(t - t')$ , and over-dots indicate time derivatives. The hard wall exerts a force  $\mathbf{F}_{\text{wall}} = -v_0 (\hat{\mathbf{v}} \cdot \hat{\mathbf{n}}) \hat{\mathbf{n}} / \mu$  if the particle is at the wall and  $\hat{\mathbf{v}} \cdot \hat{\mathbf{n}} > 0$  and zero otherwise, where  $\hat{\mathbf{n}} = \cos \psi \hat{\mathbf{x}} + \sin \psi \hat{\mathbf{y}}$  is the local normal to the wall pointing outwards; i.e., the normal component of the velocity that would drive the particle into the wall is cancelled by the wall force\*.

When the particle is at the wall, its configuration is characterized by its arclength  $s \in [0, L]$  along the boundary, where  $L$  is the box perimeter, and its orientation  $\phi = \theta - \psi$  relative to the local boundary normal (see Fig. 1). Projecting Eq. (1) onto the boundary tangent yields equations of motion for  $s$  and  $\phi$ , which hold as long as the particle stays at the wall, i.e. as long as  $|\phi| < \pi/2$ :

$$\dot{s} = v_0 \sin \phi, \quad \dot{\phi} = \xi(t) - \frac{v_0}{R(s)} \sin \phi \quad (2)$$

where  $R(s)$  is the local radius of curvature, which satisfies  $\dot{\psi} = \dot{s}/R(s)$ . We now argue that there is a “strong confinement” regime in which  $\phi$  is small. Within this regime, the particle never leaves the boundary (this would require  $|\phi| > \pi/2$ ) and its dynamics is always described by Eqs. (2), which we may linearize about  $\phi = 0$ :

$$\dot{s} = v_0 \phi, \quad \dot{\phi} = \xi(t) - \frac{v_0}{R(s)} \phi \quad (3)$$

We prove this point self-consistently, by assuming Eqs. (3) are valid and then using them to evaluate  $\phi$ . This approach is further justified by our numerical observations, see appendix A.

We first consider a circle, for which  $R(s)$  is constant and the linearized equation of motion for  $\phi$  can be directly integrated:

$$\phi(t) = \int_0^t dt' \xi(t') e^{-v_0(t-t')/R}. \quad (4)$$

It follows that  $\phi$  is a Gaussian random variable with zero mean and  $\langle \phi^2 \rangle = RD_r/v_0$ . Physically,  $\phi$  is small when the curvature radius  $R$  is much smaller than the particle’s persistence length  $v_0/D_r$ ; we refer to this case as the strong confinement limit. In the rest of this paper we consider the implications of this result for the particle density and its extension to arbitrary boxes. We only consider convex boxes for which  $R(s) > 0$  everywhere; thus  $\phi = 0$  is always a stable equilibrium point with characteristic relaxation time  $R(s)/v_0$ . The corresponding restoring force acts by moving the particle along the boundary until the wall’s normal aligns with its orientation.

### 3 Statistical Description

Let  $f(s, \phi, t)$  be the probability density of finding a particle with relative orientation  $\phi$  at arclength  $s$  at time  $t$ . Eqs. (3) can be mapped onto a Langevin equation for a free particle in one dimension with position  $s$ , velocity  $v_0 \phi$ , and position-dependent friction and temperature. Thus,  $f$  obeys an equation that has the form of the usual Fokker-Planck equation for a free particle (see, e.g., Ref. 63):

$$\partial_t f = -v_0 \phi \partial_s f + \frac{v_0}{R} \partial_\phi (\phi f) + D_r \partial_\phi^2 f \quad (5)$$

The three terms on the right-hand side of Eq. (5) describe, respectively, (i) the drift motion of a particle along its velocity  $v_0 \phi$ , (ii) the relaxation of the velocity  $v_0 \phi$  towards zero (associated with drag in the Langevin analogy), and (iii) the diffusive broadening of the velocity distribution by noise. The boundary is closed and particles leave the boundary when  $|\phi| > \pi/2$ ; therefore physical solutions satisfy  $f(s+L, \phi, t) = f(s, \phi, t)$  and  $f = 0$  for  $|\phi| \geq \pi/2$ . Since we work in the small  $\phi$  limit, we also assume  $\partial_\phi f(s, \pm\pi/2, t) = 0$ †, and seek the steady state solution to (5).

To this end, we introduce the moments  $g_n(s) = \int d\phi \phi^n f(s, \phi)$  such that  $\rho = g_0$  is the density of particles at the boundary and  $\langle \phi^n \rangle = g_n/g_0$ . The steady state solution to (5) is then obtained by solving the recurrence relation  $\partial_s g_{n+1} + \frac{n}{R} g_n - n(n-1) \frac{D_r}{v_0} g_{n-2} = 0$  (see appendix B), the first three equations of which are:

$$\partial_s g_1 = 0, \quad \partial_s g_2 + \frac{1}{R} g_1 = 0 \quad (6)$$

$$\partial_s g_3 + \frac{2}{R} g_2 - \frac{2D_r}{v_0} g_0 = 0 \quad (7)$$

† Since the Fokker-Planck equation is second order in  $\phi$ , these boundary conditions are over-constraining. Physically, however, no particle ever gets close to  $\phi = \pm\pi/2$  and thus the boundary terms are irrelevant.

\* This is the simplest choice of wall potential consistent with overdamped dynamics. It doesn’t depend on the value of  $\mu$ , which is only kept for dimensional consistency. Similar results were obtained in simulations with softer potentials.

From Eqs. (6) it follows that  $g_1$  is constant and  $g_2(s) = g_2(0) - g_1 \int_0^s du/R(u)$ . Like  $f$ ,  $g_2$  is a periodic function of  $s$ , and  $\int_0^L du/R(u) = 2\pi$  for any planar curve<sup>64</sup>; therefore  $g_1$  must be zero, i.e. there is no density flux at steady state. We close the system by neglecting  $\partial_s g_3$ . The approximation is exact for circular boxes for which  $\phi$ 's Gaussianity implies  $g_3 = 0$ , and should hold when  $R$  is nearly constant. It can also be interpreted as setting the third cumulant to zero; a standard closure method. Finally, the normalization constraint  $\int_0^L ds \rho(s) = N$  with  $N$  as the total number of particles, gives

$$\rho(s) = \frac{N}{2\pi R(s)} \quad (8)$$

$$\langle \phi^2(s) \rangle = R(s)D_r/v_0 \quad (9)$$

Eq. (8) is our primary result. The density of particles at the boundary is inversely proportional to the local curvature radius; i.e., regions of high curvature act as attractors for active particles. A more general derivation of this result can be found in appendix C. The second key result, Eq. (9), is that fluctuations in  $\phi$  are controlled by  $RD_r/v_0$ , consistent with the premise that  $\phi$  is small under strong confinement. This result is limited by the validity of our closure approximation and its scope and relevance are discussed in section 5.

## 4 Pressure

We now consider the mechanical pressure exerted locally on the boundary by the active particles, which is equal to

$$P = \rho \left\langle \frac{v_0 \hat{\mathbf{v}}}{\mu} \cdot \hat{\mathbf{n}} \right\rangle = \frac{v_0 \rho}{\mu} \langle \cos \phi \rangle \quad (10)$$

with  $v_0/\mu$  the force exerted by a single particle aligned with the normal. In the strong confinement (small noise) regime where  $\phi$  is small, we may approximate  $\cos \phi$  as 1 and use Eq. (8) to get

$$P(s) = \frac{v_0 \rho(s)}{\mu} = \frac{N v_0}{2\pi \mu R(s)} \quad (11)$$

In other words, the pressure on the boundary is proportional to the density and hence to the curvature.

To get the leading order correction to the infinite confinement (zero noise) limit, we expand the cosine in Eq. (10) to second order in  $\phi$  and use Eqs. (8)-(9):

$$P(s) = \frac{v_0 \rho(s)}{\mu} \left( 1 - \frac{1}{2} \langle \phi^2(s) \rangle \right) = \frac{N v_0}{2\pi \mu R(s)} \left( 1 - \frac{R(s)D_r}{2v_0} \right) \quad (12)$$

Note that if the box is circular, the distribution of  $\phi$  is Gaussian and we can use the exact relationship  $\langle \cos \phi \rangle = e^{-\langle \phi^2 \rangle / 2}$ <sup>‡</sup> to

get

$$P(s) = \frac{N v_0}{2\pi \mu R(s)} e^{-\frac{R(s)D_r}{2v_0}} \quad (13)$$

thus making the expansion in  $\phi$  unnecessary. Naturally, expanding the exponential in Eq. (13) leads back to Eq. (12).

The decay of pressure with  $RD_r/v_0$  at low noise was recently observed in 2D and 3D simulations of active particles in circular and spherical boxes by Mallory et al.<sup>59</sup>, who discussed various expressions including those of Eqs. (12)-(13). In particular, they measured the numerical prefactor in front of  $RD_r/v_0$  in Eqs. (12)-(13) and found 0.45 in 2D and 0.9 in 3D, consistent with our predictions 1/2 in 2D and 1 in 3D (the latter is a preliminary, unpublished result obtained by extending our analysis to 3D).

## 5 Simulations

To explore the domain of validity of our statistical theory and the physics beyond the low moment closure, we perform molecular dynamics simulations of Eq. (1). We consider  $v_0 = 1$  and various  $D_r$  in elliptical boxes with major semi-axis  $a \geq 1$  and minor semi-axis  $b = 1$  aligned with the  $x$  and  $y$  axes respectively. We plot results against the polar angle  $\alpha$  rather than the arclength; thus the curvature radius oscillates between  $R = b^2/a$  at  $\alpha = 0, \pi$  and  $R = a^2/b$  at  $\alpha = \pm\pi/2$ .

The simulation results are shown in Fig. 2. As expected, in the circular case ( $a = 1$ ) the distribution of  $\phi$  (not shown) is Gaussian and both  $\rho$  and  $\langle \phi^2 \rangle$  match the theory perfectly. Near-perfect agreement between Eq. (8) and the observed density  $\rho$  persists at all simulated aspect ratios. The magnitude and qualitative behavior of  $\langle \phi^2 \rangle$  remain well captured as well, but quantitative agreement is lost with increasing  $a$ , even though  $RD_r/v_0$  is small. This results from the breakdown of the  $\partial_s g_3 = 0$  assumption as the distribution of  $\phi$  departs from Gaussianity (see appendix D). To improve the theory, one may push the moment closure to higher orders; i.e., set the  $n^{\text{th}}$  cumulant to zero for some  $n > 3$ . This leads to a non-linear equation for  $\rho$  and  $g_2$  that involves derivatives of  $\rho$  and  $R$  with respect to  $s$ , even for  $n = 4$ . These terms suggest that the prediction  $\langle \phi^2 \rangle = RD_r/v_0$  requires not only  $RD_r/v_0 \ll 1$  but also  $dR/ds \ll 1$ , and thus may only hold in slightly deformed circular boxes.

In Fig. 3 we plot the mechanical pressure exerted on the boundary, defined by Eq. (10). At low noise, Eq. (11) closely matches the simulation results over a large range of aspect ratios. This follows from the fact that the density distributions observed in the simulations closely match Eq. (8) (see top panel of Fig. 2) and  $\phi$  is small (see bottom panel of Fig. 2). In the bottom panel of Fig. 3, we show the effect of angular noise on the pressure, described theoretically by Eqs. (12)-(13). Since our prediction relies on the prediction Eq. (9) for

<sup>‡</sup>The relationship follows from  $\langle e^{\phi} \rangle = e^{\langle \phi^2 \rangle / 2}$ , which is obtained from the Gaussian distribution's moment generating function.

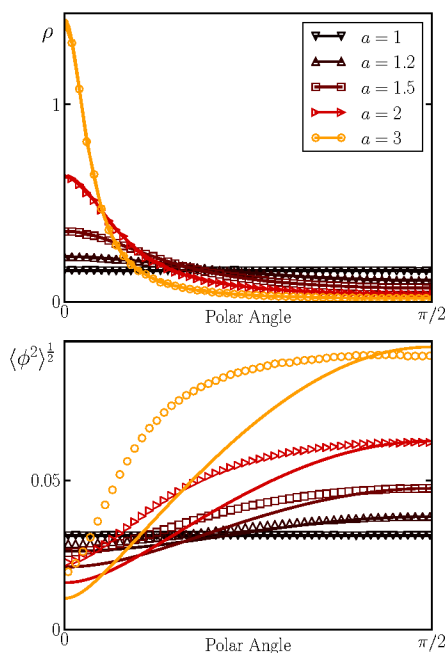


**Fig. 2** Boundary density  $\rho$  (top) and standard deviation  $\langle \phi^2 \rangle^{1/2}$  of the orientation relative to the boundary normal (bottom) as a function of polar angle in the first quadrant of elliptic boxes. The boxes have major semi-axis  $a \geq 1$  and minor semi-axis  $b = 1$ , aligned with the  $x$  and  $y$  axes respectively. Symbols are from simulations with  $D_r = 10^{-3}$ . Solid lines are from Eqs. (8)-(9). Both  $\rho$  and  $\langle \phi^2 \rangle$  are symmetric with respect to reflections about 0 and  $\pi/2$ .

the angular variance  $\langle \phi^2 \rangle$ , which as we just showed (bottom panel of Fig. 2) is only quantitatively accurate in nearly circular boxes, we restrict ourselves to such boxes. At small  $RD_r/v_0$ , the exponential form, Eq. (12), and its expansion, Eq. (13), are nearly equivalent, and both match the data. As  $RD_r/v_0$  is increased beyond the strong confinement limit, several of our assumptions break down: (i) particles start leaving the boundary, (ii) the density on the boundary is no longer proportional to  $R^{-1}$ , (iii) the variance  $\langle \phi^2 \rangle$  no longer obeys Eq. (9). These effects, however, partially cancel each other out in such a way that Eq. (13) provides a reasonable description of the evolution of the average pressure well beyond the domain of strict applicability of our theory.

To understand why the low moment closure successfully predicts  $\rho$  even when it poorly describes  $\langle \phi^2 \rangle$ , we now consider the limit case  $\phi = 0$ , or  $\theta = \psi$ , in which a particle is always located at the position  $s$  where its orientation aligns with the boundary normal. Since the dynamics of  $\theta$  is purely diffusive, its steady-state distribution is flat:  $\rho(\theta) = \rho(\psi) = N/(2\pi)$ . A change of variable then yields  $\rho(s) = (d\psi/ds)\rho(\psi) \propto 1/R$ . In other words, for sufficiently

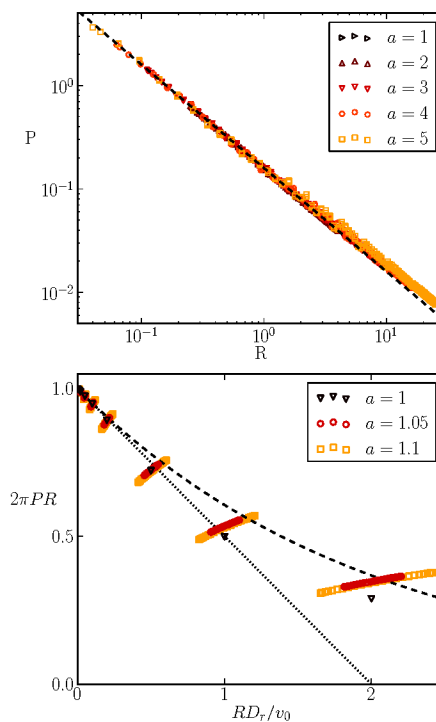


**Fig. 3** Top: Mechanical pressure  $P$  exerted by a single particle on the boundaries of ellipses of various aspect ratios  $a$  as a function of the local radius of curvature  $R(s)$  for  $D_r = 10^{-3}$ . The dashed line is the predicted pressure  $P = (2\pi R(s))^{-1}$  in the  $D_r = 0$  limit. Bottom: Pressure  $P$  normalized by its zero noise value  $(2\pi R(s))^{-1}$  as a function of the confinement parameter  $RD_r/v_0$  where  $R(s)$  is the local radius of curvature. The dotted line and the dashed line correspond to the predictions of Eqs. (12) and (13), respectively. Each run generates a cloud of data points corresponding to various locations along the boundary; the horizontal spread of the cloud results from the fact that each location monitored on the boundary has a different local radius of curvature  $R(s)$ .

small fluctuations of  $\phi = \theta - \psi$ ,  $\rho(s)$  is controlled by  $d\psi/ds$  and is essentially independent of the form of the distribution of  $\phi$ . This reasoning only requires  $\psi(s)$  to be monotonic and should apply to any convex box.

## 6 Polygonal Boxes

The previous paragraph suggests that Eq. (8) applies to arbitrary convex boxes with no restriction on the magnitude of curvature, provided  $\phi$  is small. However, under what conditions is  $\phi$  small in such a container, and do these conditions correspond to the strong confinement limit defined above? To elucidate this point, we turn to a class of shapes for which both  $R$  and  $dR/ds$  are unbounded, namely polygons.

The radius of curvature is now discontinuous, equal to in-

finiteness along the edges and zero at the corners.  $\psi(s)$  is a step function with value  $\psi_i$  on the edge connecting corners  $i$  and  $i-1$  (corner indices are defined modulo the number of corners). The dynamics at corners follows from that at edges: a particle leaves corner  $i$  along edge  $i$  (resp. edge  $i-1$ ) as soon as  $\theta > \psi_i$  (resp.  $\theta < \psi_{i-1}$ ). Conversely, a particle remains stuck at corner  $i$  as long as  $\theta \in [\psi_{i-1}, \psi_i]$ . The numerical results shown in this section were obtained with the polygonal box pictured on Fig. 1, which has a wide variety of angles and a perimeter  $L \approx 8.93$  (i.e. a radius of order one). Similar results were obtained with different boxes.

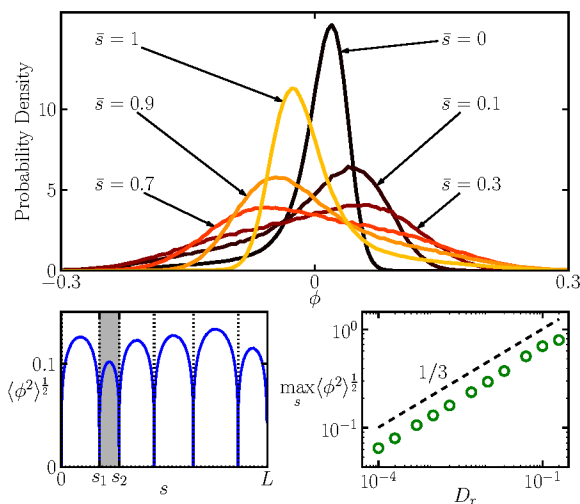


**Fig. 4** Top: Distribution of the orientation  $\phi$  relative to the boundary normal at several normalized arclengths  $\bar{s} = (s - s_1)/(s_2 - s_1)$  between corners 1 and 2 ( $\bar{s} = 0$  at corner 1,  $\bar{s} = 1$  at corner 2) of the polygon shown on Fig. 1 for  $D_r = 10^{-3}$ . Bottom left: Standard deviation of  $\phi$  as a function of arclength for  $D_r = 10^{-3}$ . The dotted lines indicate the positions of the corners. The gray area represents the region between corners 1 and 2 from which the distributions of the top panel are extracted. Bottom right: Upper bound of the standard deviation of  $\phi$  across the boundary as a function of  $D_r$ . The dashed line is a power law with slope  $1/3$  as suggested by the analysis in the text.

Because of the singular nature of curvature in a polygon, the mechanisms controlling  $\phi$  are quite different from those at work in the ellipses of section 5. In particular, the distribution of  $\phi$  is non-local, i.e. it cannot be predicted from the local geometry (the curvature and its derivatives) alone. This is clear from the top panel of Fig. 4, which shows the distribution of  $\phi$  at various points along an edge: each point has a different distribution, yet every point has the exact same local geometry (that of a straight line). The distributions are also heavily skewed, and the prediction  $\langle \phi^2 \rangle = RD_r/v_0 = \infty$  from Eq. (9) is clearly wrong.

To evaluate  $\phi$ , we need to treat corners and edges separately.

At a corner, the radius of curvature is zero and the linearized equations of motion (3) reduce to  $\dot{s} = 0$  and  $\dot{\phi} = 0$ . Physically, a particle remains stationary as long as its orientation lies between the outward normals to the two edges meeting at the corner (see bottom right panel of Fig. 1), hence  $\dot{s} = 0$ . During this time, the active force  $v_0 \hat{\mathbf{v}}$  is fully balanced by the wall force  $\mathbf{F}_{\text{wall}}$ . One can then interpret  $\phi$  as the angle between  $\hat{\mathbf{v}}$  and  $-\mathbf{F}_{\text{wall}}$ , which is well defined and equal to zero even though the normal  $\hat{\mathbf{n}}$  is ill-defined.

At an edge, the radius of curvature is infinite and the linearized equations of motion (3) reduce to  $\dot{s} = v_0 \phi$  and  $\dot{\phi} = \xi(t)$ . In the absence of boundaries, the statistical properties of  $s$  and  $\phi$  are easily derived. However, the presence of corners that can absorb and release particles makes the problem much trickier, and beyond the scope of this paper. A similar problem has been studied in the context of first-passage processes under the name “random accelerated process”, and we refer the interested reader to Refs. 65, 66 for more details on the topic. Here, we only seek to understand whether and how the angle  $\phi$  goes to zero when the box size (or the noise) goes to zero, which can be achieved using scaling arguments based on the unbounded results. To this end, we consider a particle that just left a corner located at  $s = 0$ . Since  $\phi$  is always zero while at a corner, we also have  $\dot{s} = v_0 \phi = 0$ , which completes the initial condition. We now forget about the corner and integrate the equations of motion:  $\phi(t) = \int_0^t dt' \xi(t')$  and  $s(t) = v_0 \int_0^t dt' \int_0^{t'} dt'' \xi(t'')$ , from which it follows that  $\phi$  and  $s$  are Gaussian variables with zero mean and variance  $\langle \phi(t)^2 \rangle = 2D_r t$  and  $\langle s(t)^2 \rangle = \frac{2}{3} v_0^2 D_r t^3$  respectively. The root mean squared displacement  $\langle s(t)^2 \rangle^{1/2}$  is the typical distance travelled along the edge after a time  $t$ ; the time at which it is equal to the edge length  $\ell$  provides an estimate for the time it takes a particle to cross the edge:  $t \sim \ell^{2/3} / (v_0^{2/3} D_r^{1/3})$  §. Finally, inserting this crossing time into the root mean squared angular displacement  $\langle \phi(t)^2 \rangle^{1/2} = (2D_r t)^{1/2}$  yields an estimate for the typical angle  $\phi$  reached in the course of crossing an edge of length  $\ell$ :

$$\phi \sim (\ell D_r / v_0)^{1/3} \quad (14)$$

We now show that this scaling expression can describe the fluctuations of  $\phi$  on the edges of an actual polygon by testing it against simulation data. Fig. 4 shows the square root of the angular variance  $\langle \phi^2 \rangle^{1/2}$  along the boundary of a polygon (bottom left edge) and its upper bound as a function of the angular noise strength  $D_r$  (bottom right panel). As suggested by the scaling analysis, the latter scales as  $D_r^{1/3}$ . Dimensional analysis then imposes that it in fact scales as  $(\ell D_r / v_0)^{1/3}$ , thus validating Eq. (14). The important result

§ An exact result on the mean escape time of a randomly accelerated process with absorbing boundaries leads to the same scaling<sup>65</sup>. Additionally, the scaling argument we presented here can also be found in Ref. 66.

here is that, despite the infinite radius of curvature, the amplitude  $\langle \phi^2 \rangle^{1/2}$  of the angular fluctuations does go to zero in the limit of small boxes or small noise, *i.e.* in the limit of strong confinement. However, comparing the polygonal result,  $\langle \phi^2 \rangle^{1/2} \sim (\ell D_r / v_0)^{1/3}$  where  $\ell$  is the edge length, with the result of Eq. (9),  $\langle \phi^2 \rangle^{1/2} \sim (R D_r / v_0)^{1/2}$  where  $R$  is the radius of curvature, reveals that the  $\phi = 0$  limit is harder to attain in polygonal boxes than in rounder ones.

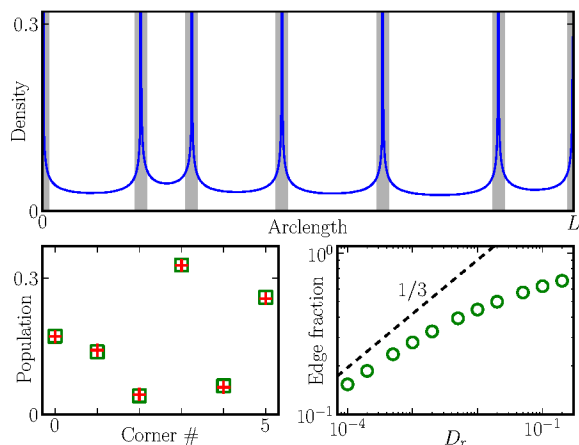


**Fig. 5** Top: Boundary density  $\rho$  as a function of arclength for the polygonal box of Fig. 1 with perimeter  $L \approx 8.93$ . Bottom left: Observed (crosses) and predicted (squares) corner populations. The former are obtained by integrating the density over each grey region of the top panel. The latter are renormalized to account for edge particles; *i.e.*, particles not in any of the grey regions. Bottom right: Fraction of edge particles as a function of the angular noise  $D_r$ . A power law with slope  $1/3$  is shown for reference. The edge fraction for the other two panels ( $D_r = 10^{-3}$ ) is 28%.

Since  $\phi$  goes to zero in the strong confinement limit, we apply the reasoning developed at the end of section 5, which results in the following expression for the density:

$$\rho(s) = \frac{d\psi}{ds} \rho(\psi) = \frac{N}{2\pi} \sum_i \beta_i \delta(s - s_i) \quad (15)$$

where  $\delta$  is the Dirac delta function,  $s_i$  is the arclength of corner  $i$ , and  $\beta_i = \psi_i - \psi_{i-1}$  is the size of the angular sector lying between the outward normals of the two edges meeting at corner  $i$  (see Fig. 1). Edges occupy a set of measure zero in the space of orientations and thus have zero population. Corner  $i$  traps every particle whose orientation  $\theta$  lies in the interval  $[\psi_{i-1}, \psi_i]$  and its population is proportional to its size  $\beta_i$ .

The simulation results are shown in Fig. 5. As expected, there are sharp density peaks at each corner (top panel), and the corner populations (the areas under these peaks) are proportional to  $\beta$  (bottom left panel). The fraction of particles not in the vicinity of any corner (the “edge fraction”), on the other

hand, decreases slowly with  $LD_r/v_0$  (bottom right panel), remaining of order 10% at  $LD_r/v_0 \sim 10^{-3}$ . This is a consequence of the slow decay of  $\phi$  as one decreases the box size or the noise (Eq. (14)). In other words, the meaning of “strong confinement” is more restrictive for polygonal boxes than for rounder ones. However, Eq. (15) accurately describes the relative corner populations even when edge fractions are large.

## 7 Conclusion

In summary, we have shown how to predict the density and pressure distribution of a simple active fluid from the geometry of its confining box, provided the box is convex and small enough. Conversely, our theory predicts the box shape that will yield any desired density profile on the boundary, thus offering the first general tool to understand and design such confinements.

The result relies on the ability of particles to circumnavigate their container faster than they re-orient (the strong confinement limit). This limit is readily achieved when curvature is positive and sufficiently large everywhere, *e.g.* in the ellipses of section 5. When the boundary has regions of very small curvature (*e.g.* the flat edges of a polygon), on the other hand, the theory is only fully accurate for extremely small box size or angular noise; otherwise it underestimates the density in the regions of very small curvature. However, the theory remains qualitatively correct over a broad region of parameter space. Furthermore, zero curvature is the worst-case scenario for a convex box. Thus, we expect the theory to apply to convex boxes of arbitrary shape, within the limitations discussed above.

## Appendix A: Bulk Fraction

Fig. 6 shows the bulk fraction – the fraction of particles not sitting at the boundary – extracted from numerical simulations in various elliptical and polygonal boxes as a function of the dimensionless confinement parameter  $\ell D_r / v_0$ , where  $\ell$  is a relevant length scale of the box. For ellipses (top panel of Fig. 6), the two available length scales are the semi-axes  $a \geq 1$  and  $b = 1$ , and dimensional analysis imposes  $\ell = a \tilde{\ell}(\frac{a}{b})$ . Our theory does not predict the form of  $\tilde{\ell}$ ; however we observe a good collapse of the bulk fraction data with a power law  $\tilde{\ell}(x) = x^{0.5}$ , *i.e.*  $\ell = a^{1.5} b^{-0.5}$ . For polygons (bottom panel of Fig. 6), the amplitude of orientation fluctuations is controlled by the length of the edges (see Eq. (14) and Fig. 4). Particles are most likely to leave the boundary on the longest edge, whose length we take as the relevant length scale  $\ell$ .

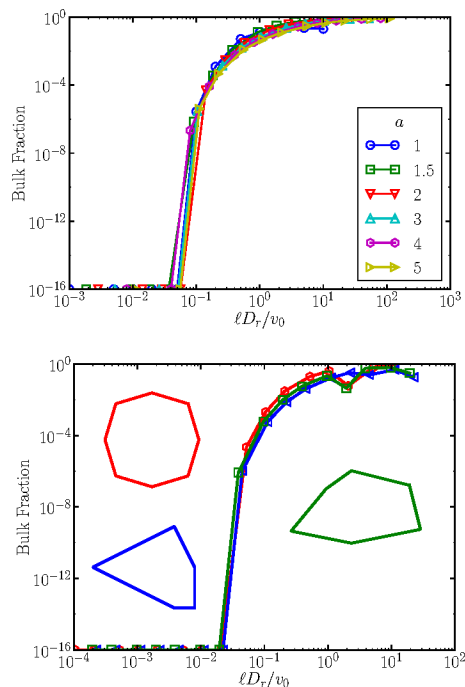


**Fig. 6** Simulated fraction of particles in the bulk as a function of the dimensionless confinement parameter  $\ell D_r/v_0$  for ellipses of various aspect ratios  $a$  (top) and for three different polygons (bottom; the polygons are shown next to the curves), where  $\ell$  is a relevant box length:  $\ell = a^{1.5}$  for ellipses, and  $\ell$  is equal to the longest edge length for polygons, as described in the text. In both cases, the bulk fraction is negligible for  $\ell D_r/v_0 \lesssim 10^{-1}$ .

## Appendix B: Moment expansion

Here we establish the recurrence relation for the moments

$$g_n(s, t) = \int d\phi \phi^n f(s, \phi, t) \quad (16)$$

from the steady-state version of the Fokker-Planck equation Eq. (5):

$$0 = -v_0 \phi \partial_s f + \frac{v_0}{R} \partial_\phi (\phi f) + D_r \partial_\phi^2 f \quad (17)$$

To this end, we multiply (17) by  $\phi^n$  and integrate over  $\phi$ :

$$0 = - \int_{-\pi/2}^{\pi/2} d\phi \phi^{n+1} \partial_s f + \frac{1}{R} \int_{-\pi/2}^{\pi/2} d\phi \phi^n \partial_\phi (\phi f) + \frac{D_r}{v_0} \int_{-\pi/2}^{\pi/2} d\phi \phi^n \partial_\phi^2 f \quad (18)$$

The spatial derivative can be taken out of the first integral on the right-hand side of Eq. (18); which then reduces to  $g_{n+1}$ . The second and third integrals can also be expressed in terms

of the moments by integrating by part once and twice respectively. The assumption  $f(\pm\pi/2) = \partial_s f(\pm\pi/2) = 0$  guarantees that all boundary terms vanish:

$$\int_{-\pi/2}^{\pi/2} d\phi \phi^n \partial_\phi (\phi f) = -n g_n \quad (19)$$

$$\int_{-\pi/2}^{\pi/2} d\phi \phi^n \partial_\phi^2 f = n(n-1) g_{n-2} \quad (20)$$

Substituting these results in Eq. (18) yields the desired recurrence relation:

$$\partial_s g_{n+1} + \frac{n}{R} g_n - n(n-1) \frac{D_r}{v_0} g_{n-2} = 0 \quad (21)$$

## Appendix C: Overdamped Approach

Here we present a derivation based on stochastic calculus of the main result of the paper: the relationship between the density on the boundary and the local curvature radius of the boundary, Eq. (8).

We start from the linearized equations of motion on the boundary Eqs. (2) (main text), written in a form that emphasizes their equivalence with a Langevin equation for a free particle with position-dependent friction and temperature:

$$\dot{v} = \dot{s}, \quad \dot{v} = -\frac{v_0}{R} v + v_0 \xi(t), \quad (22)$$

where  $v = v_0 \phi$  and  $\langle \xi(t) \xi(t') \rangle = 2D_r \delta(t-t')$ . Then, eliminating the momentum variable  $v$  (or  $\phi$ ) by averaging over the fast time scale  $R/v_0$  is equivalent to taking the overdamped limit. Since the friction coefficient is position-dependant, care must be taken to circumvent the ‘‘Ito-Stratonovitch dilemma’’. The problem was solved by Sancho et al.<sup>67</sup>, who find that  $s$  obeys the following Stratonovitch stochastic differential equation:

$$\dot{s} = R(s) \xi(t). \quad (23)$$

The corresponding Smoluchowski equation for the density  $\rho(x, t) \equiv \langle \delta(x-s(t)) \rangle$  is

$$\partial_t \rho = D_r \partial_x [R \partial_x (R \rho)], \quad (24)$$

whose steady-state solution is given by

$$\rho(x) = \frac{c_0}{R(x)} \left[ 1 + \int_0^x \frac{c_1 dy}{R(y)} \right]. \quad (25)$$

The two integration constants  $c_0$  and  $c_1$  are determined by enforcing the periodicity of  $\rho(x)$ :

$$\rho(x) = \rho(x+L) \implies \int_0^L \frac{c_1 dy}{R(y)} = 0 \implies c_1 = 0 \quad (26)$$

and the normalization of density:

$$\int_0^L dx \rho(x) = N \implies \int_0^L \frac{c_0 dx}{R(x)} = N \implies c_0 = \frac{N}{2\pi} \quad (27)$$

where we have used the relation  $\oint_0^L dx/R(x) = 2\pi$  for plane curves. The resulting expression for  $\rho$ :

$$\rho(s) = \frac{N}{2\pi R}, \quad (28)$$

is identical to that of Eq. (8), obtained by moment expansion.

## Appendix D: Angular distribution

To assess the importance of higher order moments in Eq. (7), we show in Fig. 7 the variance, skewness and kurtosis of the distribution of the angle  $\phi$  between the boundary normal and the particle's orientation in ellipses of various aspect ratios  $a$ . The data comes from the same runs used for Fig. 2. As suggested by the mismatch between the prediction  $\langle \phi^2 \rangle = RD_r/v_0$  and the numerical observations on Fig. 2 for values of  $a$  not close to 1, higher order moments can only be neglected in almost circular boxes.

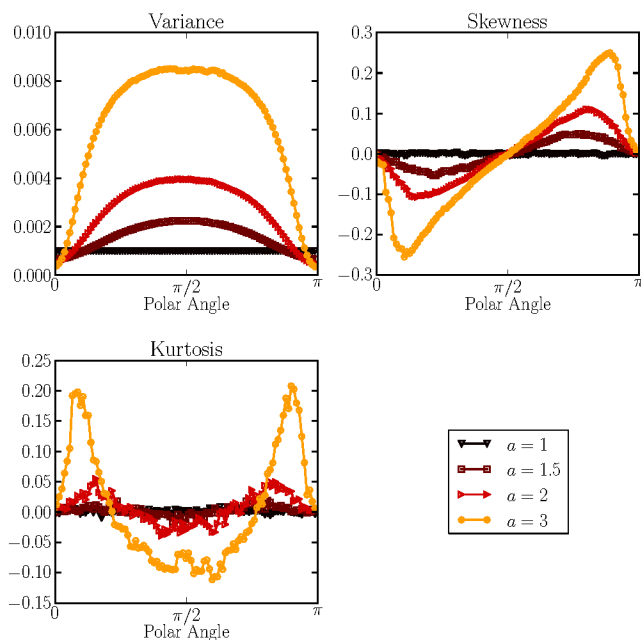


**Fig. 7** Variance, skewness and kurtosis of the orientation  $\phi$  relative to the boundary normal in small elliptical boxes of aspect ratio  $a$ .

## Acknowledgements

This research was supported by NSF-MRSEC-0820492 and NSF-DMR-1149266. Computational resources were provided

by the NSF through XSEDE computing resources and the Brandeis HPCC.

## References

- [1] V. Schaller, C. A. Weber, B. Hammerich, E. Frey and A. R. Bausch, *Proceedings of the National Academy of Sciences*, 2011, **108**, 19183–19188.
- [2] C. Dombrowski, L. Cisneros, S. Chatkaew, R. E. Goldstein and J. O. Kessler, *Phys. Rev. Lett.*, 2004, **93**, 098103 (4 pages).
- [3] F. Peruani, J. Starruß, V. Jakovljevic, L. Sjøgaard-Andersen, A. Deutsch and M. Bär, *Phys. Rev. Lett.*, 2012, **108**, 098102.
- [4] M. Poujade, E. Grasland-Mongrain, A. Hertzog, J. Jouanneau, P. Chavrier, B. Ladoux, A. Buguin and P. Silberzan, *PNAS*, 2007, **104**, 15988–15993.
- [5] X. Trepat, M. R. Wasserman, T. E. Angelini, E. Millet, D. A. Weitz, J. P. Butler and J. J. Fredberg, *Nat. Phys.*, 2009, **5**, 426–430.
- [6] M. Ballerini, N. Cabibbo, R. Candelier, A. Cavagna, E. Cisbani, I. Giardina, V. Lecomte, A. Orlandi, G. Parisi, A. Procaccini, M. Viale and V. Zdravkovic, *Proceedings of the National Academy of Sciences*, 2008, **105**, 1232–1237.
- [7] J. Palacci, C. Cottin-Bizonne, C. Ybert and L. Bocquet, *Phys. Rev. Lett.*, 2010, **105**, 088304.
- [8] W. F. Paxton, K. C. Kistler, C. C. Olmeda, A. Sen, S. K. St. Angelo, Y. Cao, T. E. Mallouk, P. E. Lammert and V. H. Crespi, *J. Am. Chem. Soc.*, 2004, **126**, 13424–13431.
- [9] Y. Hong, N. M. K. Blackman, N. D. Kopp, A. Sen and D. Velegol, *Phys. Rev. Lett.*, 2007, **99**, 178103.
- [10] H.-R. Jiang, N. Yoshinaga and M. Sano, *Phys. Rev. Lett.*, 2010, **105**, 268302.
- [11] G. Volpe, I. Buttinoni, D. Vogt, H.-J. Kummerer and C. Bechinger, *Soft Matter*, 2011, **7**, 8810–8815.
- [12] S. Thutupalli, R. Seemann and S. Herminghaus, *New Journal of Physics*, 2011, **13**, 073021.
- [13] A. Bricard, J.-B. Caussin, N. Desreumaux, O. Dauchot and D. Bartolo, *Nature*, 2013, **503**, 95–98.
- [14] V. Narayan, S. Ramaswamy and N. Menon, *Science*, 2007, **317**, 105–108.
- [15] A. Kudrolli, G. Lumay, D. Volfson and L. S. Tsimring, *Phys. Rev. Lett.*, 2008, **100**, 058001.
- [16] J. Deseigne, O. Dauchot and H. Chaté, *Phys. Rev. Lett.*, 2010, **105**, 098001.
- [17] T. Vicsek, A. Czirók, E. Ben-Jacob, I. Cohen and O. Shochet, *Phys. Rev. Lett.*, 1995, **75**, 1226.
- [18] J. Toner and Y. Tu, *Phys. Rev. Lett.*, 1995, **75**, 4326.
- [19] J. Toner, Y. Tu and S. Ramaswamy, *Annals of Physics*, 2005, **318**, 170–244.
- [20] S. Ramaswamy, R. A. Simha and J. Toner, *EPL (Europhysics Letters)*, 2003, **62**, 196.
- [21] S. Mishra and S. Ramaswamy, *Phys. Rev. Lett.*, 2006, **97**, 090602.
- [22] F. Peruani, A. Deutsch and M. Bär, *Phys. Rev. E*, 2006, **74**, 030904.
- [23] Y. Yang, V. Marceau and G. Gompper, *Phys. Rev. E*, 2010, **82**, 031904.
- [24] F. Peruani, T. Klaus, A. Deutsch and A. Voss-Boehme, *Phys. Rev. Lett.*, 2011, **106**, 128101.
- [25] H. Chaté, F. Ginelli and R. Montagne, *Phys. Rev. Lett.*, 2006, **96**, 180602.
- [26] H. Chaté, F. Ginelli, G. Grégoire, F. Peruani and F. Raynaud, *The European Physical Journal B - Condensed Matter and Complex Systems*, 2008, **64**, 451–456.
- [27] F. Peruani, F. Ginelli, M. Bär and H. Chaté, *Journal of Physics: Conference Series*, 2011, **297**, 012014.
- [28] F. Peruani and M. Bär, *New Journal of Physics*, 2013, **15**, 065009.

- [29] S. Ramaswamy, *Annu. Rev. Condens. Matter Phys.*, 2010, **1**, 323–345.
- [30] M. C. Marchetti, J. F. Joanny, S. R. Ramaswamy, T. B. Liverpool, J. Prost, M. Rao and R. A. Simha, *Rev. Mod. Phys.*, 2013, **85**, 1143.
- [31] J. Tailleur and M. E. Cates, *Phys. Rev. Lett.*, 2008, **100**, 218103.
- [32] A. G. Thompson, J. Tailleur, M. E. Cates and R. A. Blythe, *Journal of Statistical Mechanics: Theory and Experiment*, 2011, **2011**, P02029–.
- [33] Y. Fily and M. C. Marchetti, *Physical Review Letters*, 2012, **108**, 235702.
- [34] G. S. Redner, M. F. Hagan and A. Baskaran, *Phys. Rev. Lett.*, 2013, **110**, 055701.
- [35] J. Bialké, H. Löwen and T. Speck, *EPL (Europhysics Letters)*, 2013, **103**, 30008.
- [36] M. E. Cates and J. Tailleur, *EPL (Europhysics Letters)*, 2013, **101**, 20010.
- [37] J. Stenhammar, A. Tiribocchi, R. J. Allen, D. Marenduzzo and M. E. Cates, *Phys. Rev. Lett.*, 2013, **111**, 145702.
- [38] G. S. Redner, A. Baskaran and M. F. Hagan, *Phys. Rev. E*, 2013, **88**, 012305.
- [39] Y. Fily, S. Henkes and M. C. Marchetti, *Soft Matter*, 2014, **10**, 2132–2140.
- [40] J. Stenhammar, D. Marenduzzo, R. J. Allen and M. E. Cates, *Soft Matter*, 2014, **10**, 1489–1499.
- [41] R. Wittkowski, A. Tiribocchi, J. Stenhammar, R. J. Allen, D. Marenduzzo and M. E. Cates, *Scalar  $\phi^4$  field theories for active-particle phase separation*, arXiv:1311.1256, 2014, <http://arxiv.org/abs/1311.1256>.
- [42] M. B. Wan, C. J. Olson Reichhardt, Z. Nussinov and C. Reichhardt, *Phys. Rev. Lett.*, 2008, **101**, 018102.
- [43] J. Tailleur and M. E. Cates, *EPL (Europhysics Letters)*, 2009, **86**, 60002.
- [44] R. W. Nash, R. Adhikari, J. Tailleur and M. E. Cates, *Phys. Rev. Lett.*, 2010, **104**, 258101.
- [45] M. E. Cates, *Reports on Progress in Physics*, 2012, **75**, 042601.
- [46] L. Angelani, A. Costanzo and R. D. Leonardo, *EPL (Europhysics Letters)*, 2011, **96**, 68002.
- [47] P. K. Ghosh, V. R. Misko, F. Marchesoni and F. Nori, *Phys. Rev. Lett.*, 2013, **110**, 268301.
- [48] B.-q. Ai, Q.-y. Chen, Y.-f. He, F.-g. Li and W.-r. Zhong, *Phys. Rev. E*, 2013, **88**, 062129.
- [49] C. Reichhardt and C. J. Reichhardt, *Active Matter Ratchets with an External Drift*, arXiv:1308.3741, 2013, <http://arxiv.org/abs/1308.3741>.
- [50] C. Reichhardt and C. J. Reichhardt, *Active Matter Transport and Jamming on Disordered Landscapes*, arXiv:1402.3260, 2013, <http://arxiv.org/abs/1402.3260>.
- [51] A. Kaiser, H. H. Wensink and H. Löwen, *Phys. Rev. Lett.*, 2012, **108**, 268307.
- [52] A. Kaiser, K. Popowa, H. H. Wensink and H. Löwen, *Phys. Rev. E*, 2013, **88**, 022311.
- [53] P. Galajda, J. Keymer, P. Chaikin and R. Austin, *Journal of Bacteriology*, 2007, **189**, 8704–8707.
- [54] L. Angelani, R. Di Leonardo and G. Ruocco, *Phys. Rev. Lett.*, 2009, **102**, 048104.
- [55] R. Di Leonardo, L. Angelani, D. DellArciprete, G. Ruocco, V. Iebba, S. Schippa, M. P. Conte, F. Mecarini, F. De Angelis and E. Di Fabrizio, *Proceedings of the National Academy of Sciences*, 2010, **107**, 9541–9545.
- [56] A. Sokolov, M. M. Apodaca, B. A. Grzybowski and I. S. Aranson, *Proceedings of the National Academy of Sciences*, 2010, **107**, 969–974.
- [57] J. Elgeti and G. Gompper, *EPL (Europhysics Letters)*, 2013, **101**, 48003.
- [58] C. F. Lee, *New Journal of Physics*, 2013, **15**, 055007.
- [59] S. A. Mallory, A. Šarić, C. Valeriani and A. Cacciuto, *Phys. Rev. E*, 2014, **89**, 052303.
- [60] A. Guidobaldi, Y. Jeyaram, I. Berdakin, V. V. Moshchalkov, C. A. Condat, V. I. Marconi, L. Giojalas and A. V. Silhanek, *Phys. Rev. E*, 2014, **89**, 032720.
- [61] X. Yang, M. L. Manning and M. C. Marchetti, *Aggregation and Segregation of Confined Active Particles*, arXiv:1403.0697, 2014, <http://arxiv.org/abs/1308.3741>.
- [62] B. A. Camley and W.-J. Rappel, *Velocity alignment leads to high persistence in confined cells*, arXiv:1405.7088, <http://arxiv.org/abs/1405.7088>.
- [63] H. Risken, *The Fokker-Planck Equation: Methods of Solution and Applications*, Springer Berlin Heidelberg, 1996.
- [64] R. D. Kamien, *Rev. Mod. Phys.*, 2002, **74**, 953–971.
- [65] J. Masoliver and J. M. Porrà, *Phys. Rev. Lett.*, 1995, **75**, 189–192.
- [66] S. Redner, *A Guide to First-Passage Processes*, Cambridge University Press, 2001.
- [67] J. Sancho, M. Miguel and D. Dürr, 1982, **28**, 291–305–.

## Graphical Abstract

Confinement of active particles dramatically alters their spatial distribution and mechanical properties .

